Weaker nematic phase connected to the first order antiferromagnetic phase transition in $SrFe_2As_2$ compared to $BaFe_2As_2$

David W. Tam,[1] Weiyi Wang,[1] Li Zhang,[2,1,*] Yu Song,[1] Rui Zhang,[1] Scott V. Carr,[1] H. C. Walker,[3] Toby G. Perring,[3] D. T. Adroja,[3,4] and Pengcheng Dai[1,†]

[1]*Department of Physics and Astronomy, Rice University, Houston, Texas 77005, USA*
[2]*Department of Physics, China Jiliang University, Hangzhou 310018, China,*
[3]*ISIS Facility, Rutherford Appleton Laboratory, Chilton, Didcot, Oxfordshire OX11 0QX, UK*
[4]*Highly Correlated Matter Research Group, Physics Department, University of Johannesburg, P.O. Box 524, Auckland Park 2006, South Africa*

(Received 12 November 2018; revised manuscript received 24 February 2019; published 25 April 2019)

Understanding the nature of the electronic nematic phase in iron pnictide superconductors is important for elucidating its impact on high-temperature superconductivity. Here we use transport and inelastic neutron scattering to study spin excitations and in-plane resistivity anisotropy in uniaxial pressure detwinned $BaFe_2As_2$ and $SrFe_2As_2$, the parent compounds of iron pnictide superconductors. While $BaFe_2As_2$ exhibits weakly first-order tetragonal-to-orthorhombic structural and antiferromagnetic (AF) phase transitions below $T_s > T_N \approx 138$ K, $SrFe_2As_2$ has strongly coupled first-order structural and AF transitions below $T_s = T_N \approx 210$ K. We find that the direct signatures of the nematic phase persist to lower temperatures above the phase transition in the case of $SrFe_2As_2$ compared to $BaFe_2As_2$. Our findings support the conclusion that the strongly first-order nature of the magnetic transition in $SrFe_2As_2$ weakens the nematic phase and resistivity anisotropy in the system.

DOI: 10.1103/PhysRevB.99.134519

I. INTRODUCTION

The parent compounds of iron-based superconductors such as $BaFe_2As_2$ and $SrFe_2As_2$ exhibit antiferromagnetic (AF) order below the phase transition temperature T_N [1–3]. At temperatures coinciding with or slightly above T_N, these materials also exhibit a tetragonal-to-orthorhombic structural transition at T_s, where the underlying lattice changes from having fourfold (C_4) above T_s to twofold (C_2) rotational symmetry below T_s [2,3]. In the temperature regime below T_s and above T_N, an electronic nematic phase, which breaks the orientational but not the translational symmetry of the underlying lattice [4], has been predicted [5,6]. As the nematic phase and associated fluctuations can act to enhance electron Cooper pairing for superconductivity [7–10] and are expected to play an important role in iron pinctides [11], it is important to elucidate its microscopic origin. However, in the unstrained state, $BaFe_2As_2$ and $SrFe_2As_2$ form twinned domains below T_s, making it impossible for a bulk probe to determine the intrinsic electronic properties of the individual domains or the associated nematic fluctuations. By applying uniaxial pressure along one of the orthorhombic lattice directions, one can detwin $BaFe_2As_2$ single crystals and therefore measure the intrinsic electronic anisotropy present in the orthorhombic phase [12]. When the material is completely detwinned, the magnetic Bragg peaks from the collinear AF order below T_N will appear at the in-plane $\mathbf{Q}_{AF} = (\pm 1, 0)$ wave vectors in reciprocal space, with no observable peaks at $(0, \pm 1)$ from the extinguished domain [Figs. 1(a) and 1(b)] [13–15]. As a result of this technique, one can then examine the material at temperatures above T_N to elucidate the microscopic nature of the nematic phase.

From the temperature dependence of the in-plane resistivity anisotropy measured on uniaxial pressure detwinned $BaFe_2As_2$, the electronic nematic phase has been identified to persist to a characteristic temperature T^* higher than the expected nematic ordering temperature T_s [16,17]. In previous transport and inelastic-neutron-scattering studies of uniaxial pressure detwinned $BaFe_2As_2$ [18–22], resistivity anisotropy in the paramagnetic phase above T_s is found to be associated with anisotropy in spin excitations between the AF wave vector $\mathbf{Q}_{AF} = (\pm 1, 0)$ and the disallowed wave vector $\mathbf{Q} = (0, \pm 1)$, thus suggesting that the nematic phase is driven by magnetism [23] instead of orbital ordering [24–26]. For $BaFe_2As_2$, which has separate weakly first-order magnetic and second-order structural phase transitions ($T_s > T_N$ by $\sim$0.75 K) [14], one would expect that critical spin fluctuations from the AF phase transition extend to temperatures well above T_N. On the other hand, for $SrFe_2As_2$, which has strongly coupled first-order magnetic and structural phase transitions ($T_s = T_N$) [27,28], there should not be much critical scattering above T_N. If nematic fluctuations in the paramagnetic state of iron pnictides are indeed from anisotropic spin excitations [11], one would expect the resistivity and spin-excitation anisotropy for $BaFe_2As_2$ to be considerably different from those of $SrFe_2As_2$, given the strongly first-order nature of the coupled structural and magnetic phase transitions [27,28]. Although previous transport measurements on detwinned $SrFe_2As_2$ appear to bear this out [29], there are no systematic studies to compare the resistivity and spin-excitation anisotropy in the nearly 100% detwinned $BaFe_2As_2$ and $SrFe_2As_2$.

*lzhang@cjlu.edu.cn
†pdai@rice.edu

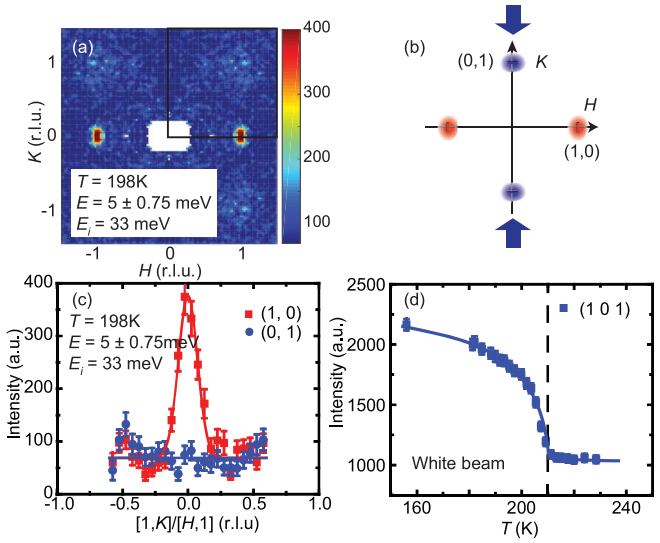

FIG. 1. Summary of the inelastic-neutron-scattering results on uniaxial pressure detwinned $SrFe_2As_2$. (a) Spin waves at an energy transfer $E = 5 \pm 0.75$ meV from a ~100% detwinned $SrFe_2As_2$ below T_N, where magnetic intensity is at $\mathbf{Q}_{AF} = (\pm 1, 0)$ and absent at $(0, \pm 1)$. (b) Reciprocal space of $SrFe_2As_2$ with twin domains. The blue and red dots mark the magnetic Bragg peak positions for the two twin domains. When uniaxial pressure is applied along the b-axis direction, only Bragg peaks and spin waves from the red domain are present. (c) Cuts of $E = 5 \pm 0.75$ meV spin waves along the red and blue positions in reciprocal space at $T = 198$ K ($<T_N$). The absence of magnetic scattering at $(0, \pm 1)$ indicates that the sample is essentially 100% detwinned. (d) Temperature dependence of the magnetic Bragg peak's intensity at $\mathbf{Q}_{AF} = (1, 0, 1)$. Note that T_N is increased under uniaxial pressure.

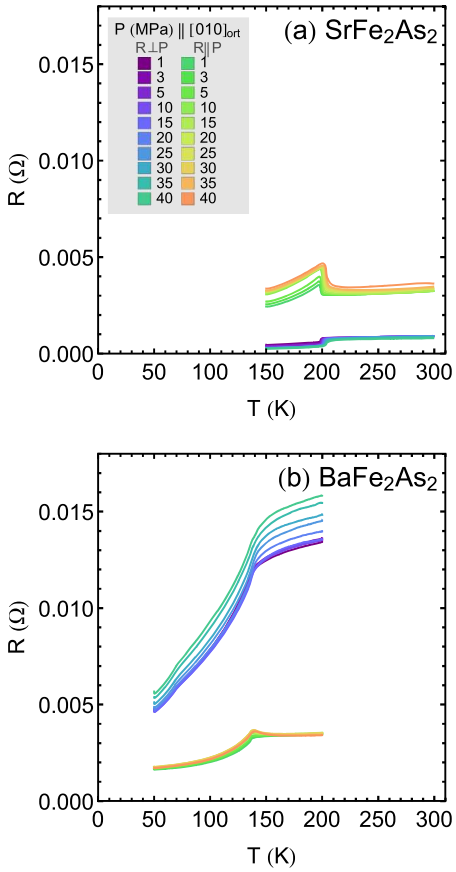

FIG. 2. Resistance $[R(\Omega)]$ of (a) $SrFe_2As_2$ and (b) $BaFe_2As_2$ obtained using a custom built uniaxial device for all pressures and temperatures. Resistance perpendicular $[R(\Omega) \perp P]$ and along $[R(\Omega) || P]$ the uniaxial pressure directions are clearly marked.

In this paper, we report transport and inelastic-neutron-scattering measurements designed to study the impact of the strongly first-order AF phase transition of $SrFe_2As_2$ on the resistivity and spin-excitation anisotropy in the paramagnetic phase. Similar to previous work [30,31], we used a mechanical uniaxial pressure device to detwin multiple samples of $SrFe_2As_2$ for inelastic-neutron-scattering experiments, and compare this to resistivity measurements as a function of carefully controlled uniaxial pressure (constant stress) using a homebuilt instrument [32]. In the unstrained state, $SrFe_2As_2$ undergoes strongly first-order coupled structural and magnetic phase transitions at $T_s = T_N \approx 210$ K from a paramagnetic tetragonal state to an AF orthorhombic state [15]. Applying fixed uniaxial pressure along the orthorhombic b axis, we find no low-energy spin excitations at disallowed positions $\mathbf{Q} = (0, \pm 1)$ [Figs. 1(a) and 1(c)], and conclude that the $SrFe_2As_2$ single crystal is nearly 100% or completely detwinned. Our inelastic-neutron-scattering experiments reveal that the spin-excitation anisotropy in the paramagnetic state, defined as $(I_{10} - I_{01})/(I_{10} + I_{01})$ where I_{10} and I_{01} are spin-excitation intensities at $\mathbf{Q}_{AF} = (\pm 1, 0)$ and $\mathbf{Q} = (0, \pm 1)$, respectively, is dramatically different for $SrFe_2As_2$ and $BaFe_2As_2$. In particular, the anisotropy above T_N is smaller and decays more rapidly in $SrFe_2As_2$ compared with measurements on $BaFe_2As_2$ under the same experimental conditions (Fig. 2). To explore the connection with the electronic nematic phase, we overlay the resistivity anisotropy in the paramagnetic state of detwinned $SrFe_2As_2$ and $BaFe_2As_2$ at several uniaxial pressures in Fig. 3. We find that the nematic phase, as revealed by pressure-induced resistivity anisotropy, also persists to a higher T/T_N in $BaFe_2As_2$ compared to $SrFe_2As_2$, independent of how the data are analyzed. Since our $BaFe_2As_2$ and $SrFe_2As_2$ single crystals are prepared the same way [33], any impurity scattering in these two materials should be similar. Since the uniaxial pressure-induced lattice distortions are similar in both materials seen in previous neutron Larmor diffraction experiments [30], we conclude that the differences in the resistivity anisotropy must be the intrinsic properties of these materials. Since in linear response regime the electronic nematic order parameter (seen either in resistivity or spin excitation anisotropy) is proportional to the pressure-induced lattice distortion [30], the different resistivity anisotropies despite similar lattice distortions mean a different nematic susceptibility in $BaFe_2As_2$ and $SrFe_2As_2$. Whereas the nematic susceptibility diverges at T_N in $BaFe_2As_2$, it does not diverge in $SrFe_2As_2$ (Fig. 3). Therefore, the resistivity anisotropy and nematic phase in the paramagnetic phase of iron pnictides are intimately associated with the nature of the magnetic phase transition and anisotropic spin excitations, consistent with expectations that the nematic phase is spin driven [11].

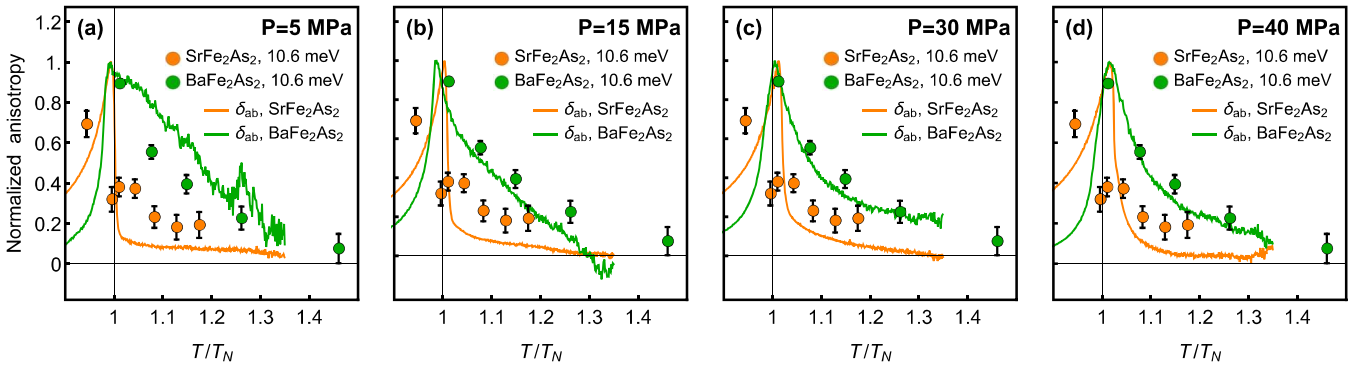

FIG. 3. T/T_N dependence of the resistivity anisotropy δ_{ab} at in-plane uniaxial pressures of (a) $P = 5$ MPa, (b) $P = 15$ MPa, (c) $P = 30$ MPa, and (d) $P = 40$ MPa for detwinned $BaFe_2As_2$ and $SrFe_2As_2$, compared to spin excitation anisotropy $(I_{10} - I_{01})/(I_{10} + I_{01})$ for detwinned $BaFe_2As_2$ and $SrFe_2As_2$, measured at $E = 10.6 \pm 2.8$ meV with incident neutron energy $E_i = 80$ meV. Below $P \approx 15$ MPa, the finite twinning of the samples obscures the connection to spin-excitation anisotropy, but for 30 and 40 MPa the connection is robust. The data for $SrFe_2As_2$ show sharp changes across T_N, indicative of the first-order nature of the transition, and similar but broader features in $BaFe_2As_2$. The large differences in spin-excitation anisotropy very close to T_N for these two materials may arise from their different low-temperature spin-anisotropy gaps [51–53].

II. EXPERIMENTAL RESULTS

A. Transport measurements

We first describe our transport measurements on detwinned $BaFe_2As_2$ and $SrFe_2As_2$ using a custom-built uniaxial detwinning instrument in a Quantum Design Dynacool physical property measurement system [32]. Single crystals of $BaFe_2As_2$ and $SrFe_2As_2$ were grown using the self-flux method [33], aligned and cut into square shapes along the orthorhombic axes, with pressure applied along an edge (the orthorhombic b axis). The pressure is directly measured throughout the experiment using a load cell which is fed back to the controller to maintain constant force [32]. Figures 2(a) and 2(b) show temperature dependence of the resistivity of $SrFe_2As_2$ and $BaFe_2As_2$, respectively. The resistance along the a- and b-axis directions for different values of uniaxial pressure is shown as a function of T/T_N, with data collected with current perpendicular (or parallel) to the pressure direction (Fig. 2). The data shows somewhat different values for the four sets of measurements (two samples, two directions) due to the small size differences between the samples. The largest source of error in the applied pressure is the estimate of the cross-sectional size of the samples, which is approximately $5.5 \times 0.4 = 2.0$ mm^2 for $SrFe_2As_2$ and $4.3 \times 0.7 = 3.0$ mm^2 for $BaFe_2As_2$, with approximately 10–20% error. In each measurement, the pressure is applied at high temperature before cooling across the phase transition, and data is collected on warming at a fixed rate. The samples were held in the uniaxial instrument between aluminum plates coated with a thin layer of Loctite E-30UT epoxy to serve as a buffer layer for even distribution of force over the sample edges. Wires were attached near the corners of the square face to measure resistivity anisotropy by the Montgomery method [20] and the direction of current/voltage was alternated between the a and b axes during the course of each temperature sweep. In this geometry, the uniaxial instrument can apply pressures between near zero and about 150 MPa for samples of these size, enough to cover the range of pressures necessary to fully detwin the crystals (∼10 MPa) and well above the pressure that causes them to break.

We choose three methods of normalizing the raw data to proceed with analysis: (1) where the raw resistance data is scaled to the value at $P = 1$ MPa and the maximum temperature (300 K for $SrFe_2As_2$ and 200 K for $BaFe_2As_2$, which is approximately $1.5T_N$ in both cases), (2) where the raw resistance data is scaled to the value at maximum temperature ($T/T_N \approx 1.5$) for each pressure independently, and (3) where the raw resistance data is scaled at $T/T_N = 1.2$ for each pressure. In each case, it is clear that the anisotropy persists to higher relative temperature in the case of $BaFe_2As_2$. Figure 3 summarizes T/T_N dependence of the normalized resistivity anisotropy δ_{ab} under different uniaxial pressure using method (2), compared to the spin excitation anisotropy.

In Fig. 4, we use method (1) for normalization, which is to the value measured at the smallest pressure and the highest temperature (approximately 1.5 T/T_N in both cases). In Figs. 4(a) and 4(b), the first set of temperature sweeps (colors between purple and blue) show normalized resistance $\tilde{R}$ perpendicular to the pressure direction (the a-axis direction R_a), and the second data (green to orange) parallel to pressure (the b-axis direction R_b). Figures 4(c) and 4(d) show the same data with the lowest pressure data subtracted, yielding the intrinsic pressure effect, which for pressures less than $P = 15$ MPa is a combination of detwinning and perturbative effects on the electronic structure. Above $P = 15$ MPa, we find no major qualitative changes for pressure above ∼15 MPa in both compounds, corresponding to complete detwinning under this pressure. The remainder of the changes are associated with the uniaxial distortion in a single domain in the case of $BaFe_2As_2$ [32] and we expect the same for $SrFe_2As_2$. For example, T_N gradually shifts upward with increasing pressure, as in the case of $BaFe_2As_2$ [32], and broadens somewhat for each sample, consistent with a small distribution of uniaxial pressure over the entire sample volume. (We note that in our data, the resistance of $BaFe_2As_2$, R_a, seems to be accumulating an offset with increasing pressure. Since its value is

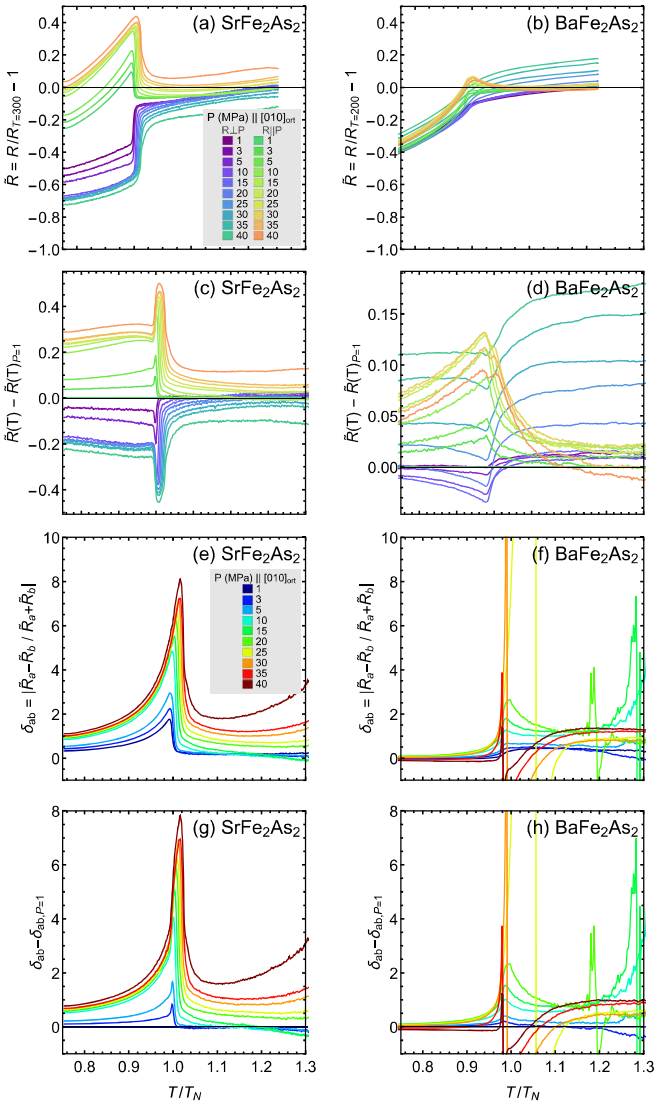

FIG. 4. Resistance and resistance anisotropy of $SrFe_2As_2$ and $BaFe_2As_2$. Normalized resistance $\tilde{R} = (R[T,P] - R[T_{\max},P=1])/R[T_{\max},P=1]$, i.e., normalized to the value at $P = 1$ MPa, $T = 300$ K for (a) $SrFe_2As_2$ or 200 K for (b) $BaFe_2As_2$. (c), (d) Uniaxial pressure effect on the normalized resistance, $\Delta_P\tilde{R} = \tilde{R}[T,P] - \tilde{R}[T,P=1]$. (e), (f) Anisotropy $\delta_{ab}[T,P] = |\Delta_P\tilde{R}_a - \Delta_P\tilde{R}_b|/(\Delta_P\tilde{R}_a + \Delta_P\tilde{R}_b)$ of the pressure-induced resistivity changes between a and b orthorhombic axes. (g), (h) Uniaxial pressure effect on the anisotropy, $\delta_{ab}[T,P] - \delta_{ab}[T,P=1]$.

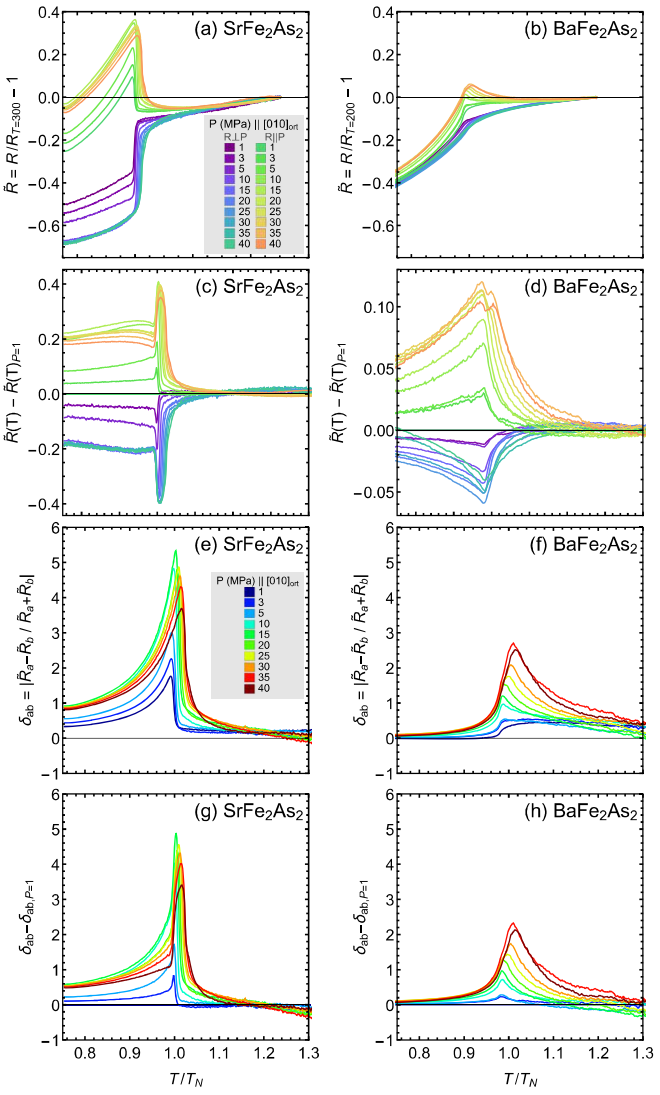

FIG. 5. Resistance and resistance anisotropy of $SrFe_2As_2$ and $BaFe_2As_2$, with the same panels as Fig. 4. Here, in (a) and (b), we use the normalized resistance $\tilde{R} = (R[T,P] - R[T_{\max},P])/R[T_{\max},P]$, i.e., normalized to the value at $T = 300$ K ($SrFe_2As_2$) or 200 K ($BaFe_2As_2$) measured at each pressure.

constant with respect to temperature, we believe this offset is extrinsic to the sample, and in methods (2) and (3) it is automatically eliminated by the normalization. Nevertheless, we proceed with method (1) under the assumption that it is intrinsic, for the sake of argument.) Figures 4(e) and 4(f) show the absolute value of anisotropy between R_a and R_b, $\delta_{ab}[T,P] = |\Delta_P\tilde{R}_a - \Delta_P\tilde{R}_b|/(\Delta_P\tilde{R}_a + \Delta_P\tilde{R}_b)$. To remove any ambiguity arising from the intrinsic temperature dependence of the resistivity, we also show in Figs. 4(g) and 4(h) the anisotropy after subtracting the anisotropy measured at the lowest pressure, $P = 1$ MPa. In principle, this extra step is not necessary since for a fully twinned crystal the anisotropy should be indistinguishable between R_a and R_b. The fact that the anisotropy is nonzero below T_N at only 1 MPa in both crystals may reflect the fact that the pressure is applied at high temperature before cooling across T_s, so even a small symmetry-breaking force can have relatively large changes on the volume fraction of different twin domains. Since there are multiple crossing points in the pressure-subtracted data [Figs. 4(c) and 4(d)], the anisotropy [Figs. 4(e) and 4(f)] contains divergencelike features in $BaFe_2As_2$ for most pressures where the values of R_a and R_b accidentally cross. However, by comparing the relatively low-pressure data such as at 10 and 15 MPa, we can clearly see that the pressure-induced resistivity anisotropy extends to a much larger T/T_N compared with that of $SrFe_2As_2$, indicating that temperature regime of the nematic phase is sensitive to the first-order nature of the AF phase transition in $SrFe_2As_2$.

In Fig. 5, we now use method (2), normalizing each temperature sweep to its highest value (approximately 1.5 T/T_N

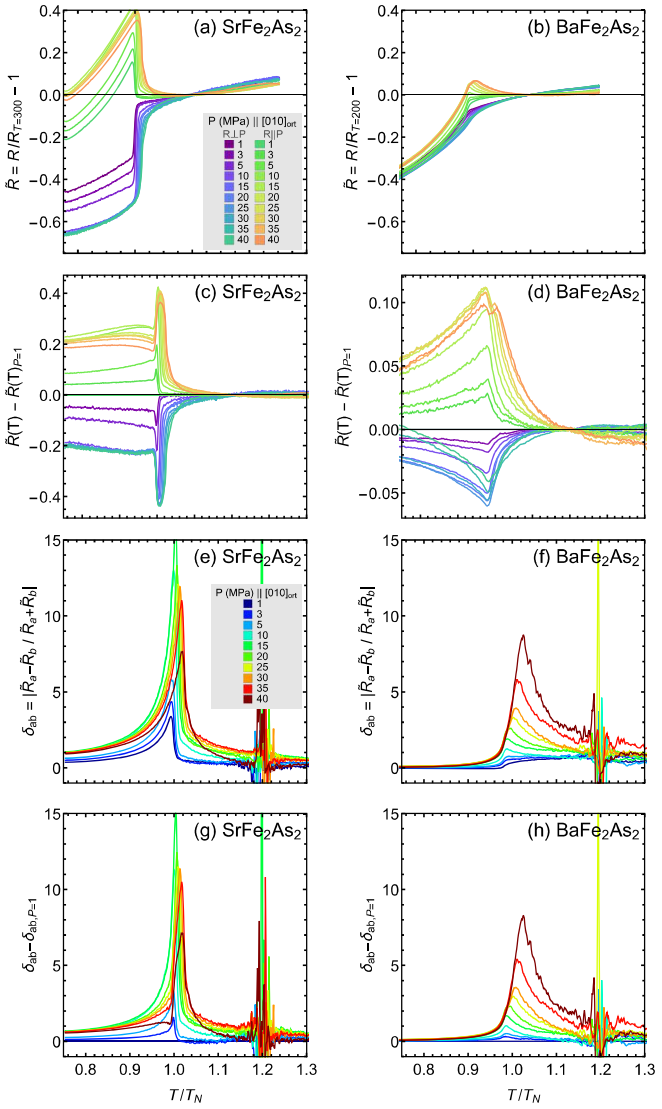

FIG. 6. Resistance and resistance anisotropy of $SrFe_2As_2$ and $BaFe_2As_2$, with the same panels as Fig. 4. Here, in (a) and (b), we use the normalized resistance $\tilde{R} = (R[T,P] - R[T = 1.2T_N, P])/R[T = 1.2T_N, P]$, i.e., normalized to the value at $T = 238$ K ($SrFe_2As_2$) or 166 K ($BaFe_2As_2$) measured at each pressure.

in both cases). This method accounts for overall changes in resistivity with increasing pressure and therefore nullifies any instrumental effects or changes caused by, for example, a small flake breaking off near one of the electrical leads. This method most clearly shows the pressure-induced anisotropy [Figs. 5(e)–5(h)] and convincingly demonstrates that the pressure effect persists to a higher T/T_N in $BaFe_2As_2$.

Finally, in Fig. 6, we use method (3), normalizing to the value at $T = 1.2T_N$ in each temperature sweep. This accounts for any possible differences in anisotropy between the compounds that may be related to temperature-induced disorder effects. Nevertheless, we recover the same conclusion that the anisotropy decays more rapidly in $SrFe_2As_2$ compared to $BaFe_2As_2$.

We make particular note here about the values chosen for T_N, since it has a measurable impact on the data in this case. In particular, we find a lower $T_N \sim 199$ K for $SrFe_2As_2$ compared with the values shown in the main text from neutron scattering $T_N \sim 210$ K. We believe the values chosen are correct in both cases, and that the uniaxial pressure is actually much higher in the samples used for neutron scattering such that the ordering temperature is increased by about 10 K. The increase in ordering temperature under pressure is a well-known effect, and is seen clearly in the present data.

Finally, we point out we have not normalized the anisotropy in these figures, except in Fig. 3. We believe the non-normalized anisotropy is a good measure of the intrinsic resistivity anisotropy under constant strain, since the lattice anisotropy under 30 MPa is known to be similar between $SrFe_2As_2$ and $BaFe_2As_2$ [30].

B. Inelastic-neutron-scattering measurements

To see if the temperature dependence of the spin excitation anisotropy in $SrFe_2As_2$ follows that of the resistivity anisotropy, we measured low-energy spin excitations across T_N with inelastic-neutron-scattering experiments performed at the MERLIN time-of-flight neutron-scattering spectrometer at ISIS, Rutherford Appleton Laboratory [34]. The single crystals were detwinned under uniaxial pressures of at least 30 MPa. We define the wave vector $\mathbf{Q}$ in three-dimensional reciprocal space in Å^{-1} as $\mathbf{Q} = H\mathbf{a}^* + K\mathbf{b}^* + L\mathbf{c}^*$, where H, K, and L are Miller indices and $\mathbf{a}^* = \hat{\mathbf{a}}2\pi/a$, $\mathbf{b}^* = \hat{\mathbf{b}}2\pi/b$, $\mathbf{c}^* = \hat{\mathbf{c}}2\pi/c$ are reciprocal lattice units (r.l.u.) [Fig. 1(b)]. In the low-temperature AF orthorhombic phase of $SrFe_2As_2$, $a \approx 5.57$ Å, $b \approx 5.51$ Å, and $c \approx 12.29$ Å [15]. The sample array was aligned with the c axis along the incident beam direction ($\mathbf{k_i} \parallel c$) with neutron energy of $E_i = 80$ meV. We carried out measurements at many temperatures above and below T_N to obtain temperature dependence of I_{10} and I_{01} for comparison with $BaFe_2As_2$ [31].

In the AF ordered state, spin waves from the collinear AF order should stem from $\mathbf{Q}_{AF} = (\pm 1, 0)$ with $L = \pm 1, \pm 3$ in reciprocal space [Fig. 1(b)] [19]. On warming to the paramagnetic phase, the scattering should have very weak L-dependence [31]. Figures 7(a) and 7(b) show spin waves of energy transfer $E = 10.6 \pm 2.8$ meV and the corresponding cuts along the $[H, 1]/[1, K]$ directions at $T = 0.94T_N$. As expected, we find spin waves at $\mathbf{Q}_{AF} = (\pm 1, 0)$ dominating the scattering and very weak magnetic scattering at $(0, \pm 1)$, consistent with the nearly 100% detwinning ratio shown in Fig. 1(c). On warming to $T = 1.01T_N$, we see a significant reduction in the spin-excitation anisotropy at $\mathbf{Q}_{AF} = (\pm 1, 0)$ (I_{10}) and $(0, \pm 1)$ (I_{01}) [Figs. 7(c) and 7(d)]. On further warming to $T = 1.18T_N$, we find that spin excitations at $\mathbf{Q}_{AF} = (\pm 1, 0)$ and $(0, \pm 1)$ almost become equal in intensity, but have weak temperature dependence. These results thus suggest that the remaining spin excitation anisotropy is due to the presence of uniaxial pressure [Figs. 7(e) and 7(f)]. Figure 7(g) shows temperature dependence of the spin excitation intensity at $\mathbf{Q}_{AF} = (\pm 1, 0)$ (I_{10}) and $(0, \pm 1)$ (I_{01}). Since the widths of the spin excitations change smoothly across T_N as shown in Fig. 7(h), we conclude that the spin excitation anisotropy at $E = 10.6 \pm 2.8$ meV reduces dramatically across T_N.

Having examined the spin excitation anisotropy above T_N at low energies just above the spin-wave gap, we turn to the energy dependence at a higher energy transfer $E = 45 \pm 5$ meV, which is about 25% of the total magnetic

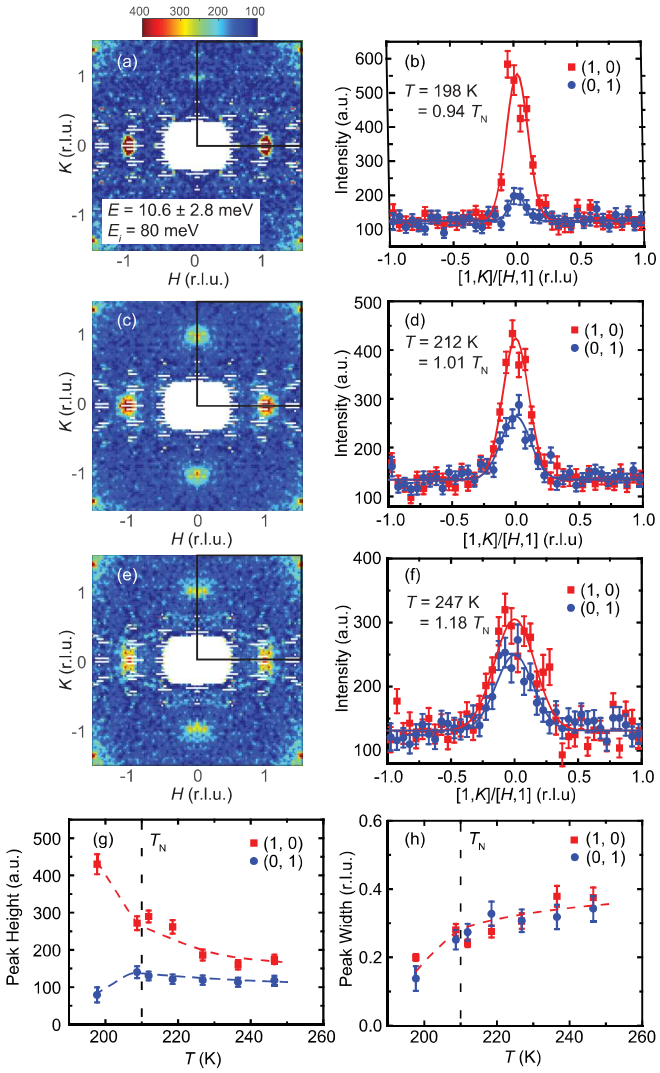

FIG. 7. Temperature dependence of the spin-excitation anisotropy as a function of increasing temperature across T_N for $SrFe_2As_2$. (a), (b) Spin waves of an energy transfer $E = 10.6 \pm 2.8$ meV at $T = 0.94T_N$ in the $[H, K]$ plane, and cuts along the $[H, 1]$ and $[1, K]$ directions. Identical scans at (c), (d) $T = 1.01T_N$, and (e), (f) $T = 1.18T_N$. (g) Temperature dependence of the peak intensity at I_{10} and I_{01} across T_N. (h) Temperature-dependent width of spin excitations across T_N for $SrFe_2As_2$.

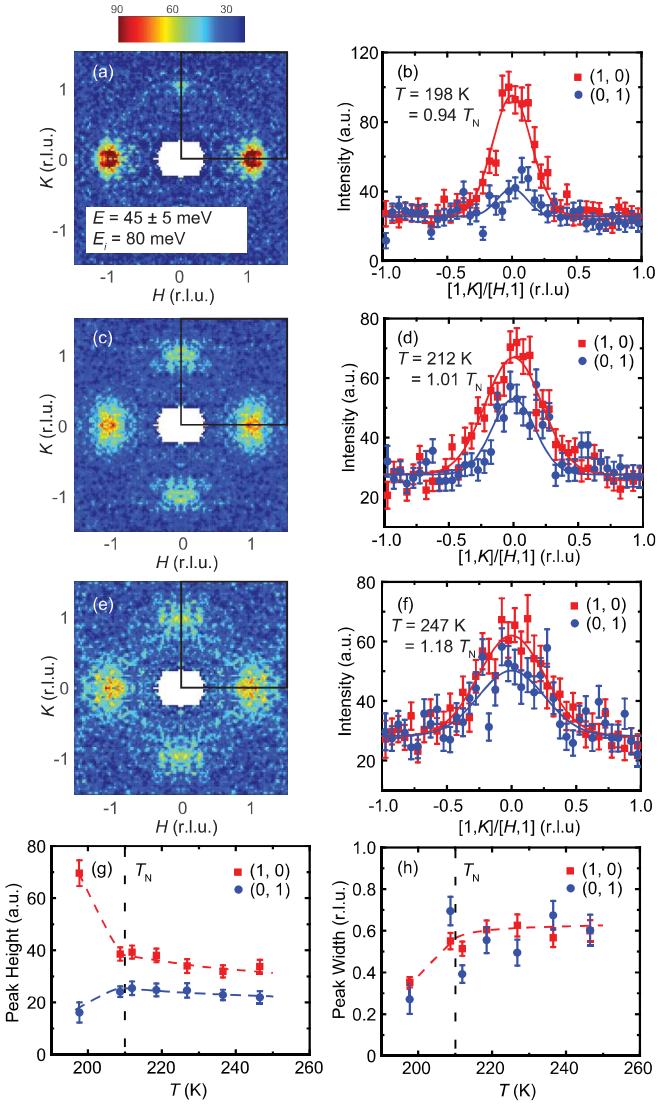

FIG. 8. Temperature dependence of the spin-excitation anisotropy at an energy transfer of $E = 45 \pm 5$ meV as a function of increasing temperature across T_N for $SrFe_2As_2$. (a), (b) Spin waves of $E = 45 \pm 5$ meV at $T = 0.94T_N$ in the $[H, K]$ plane, and cuts along the $[H, 1]$ and $[1, K]$ directions. The excitation anisotropy is somewhat smaller than that at $E = 10.6 \pm 2.8$ meV. Identical scans at (c), (d) $T = 1.01T_N$, and (e), (f) $T = 1.18T_N$. (g) Temperature dependence of the peak intensity at I_{10} and I_{01} across T_N. The persistent spin-excitation anisotropy above T_N is due to the presence of uniaxial pressure, similar features are also seen in $BaFe_2As_2$. (h) Temperature-dependent width of spin excitations across T_N for $SrFe_2As_2$.

bandwidth. At $T = 0.94T_N$, we also see clear spin-wave anisotropy with most of the spectral weight at $\mathbf{Q}_{AF} = (\pm 1, 0)$, quite similar to spin waves at $E = 10.6 \pm 2.8$ meV [Figs. 8(a) and 8(b)]. On warming to $T = 1.01T_N$, spin excitations at $\mathbf{Q}_{AF} = (\pm 1, 0)$ and $(0, \pm 1)$ are still anisotropic [Figs. 8(c) and 8(d)], but much less so compared with data at $E = 10.6 \pm 2.8$ meV [Figs. 7(c) and 7(d)]. Finally, we see very little spin-excitation anisotropy at $T = 1.18T_N$ [Figs. 8(e) and 8(f)], very similar to the data at $E = 10.6 \pm 2.8$ meV [Figs. 7(e) and 7(f)]. Figures 8(g) and 8(h) show the temperature dependence of the magnetic scattering intensity and width of the spin excitations, respectively, at $\mathbf{Q}_{AF} = (\pm 1, 0)$ and $(0, \pm 1)$.

To quantitatively summarize the spin-excitation anisotropy in the paramagnetic state of $SrFe_2As_2$ and $BaFe_2As_2$, we plot in Fig. 3 the relative temperature (T/T_N) dependence of the spin-excitation anisotropy at low energy for these two materials under nearly 100% detwinning, next to the resistivity anisotropy measured on our uniaxial instrument. In the paramagnetic state, we see a clear difference in the temperature dependence of the spin excitation anisotropy at an energy transfer $E = 10.6 \pm 2.8$ meV, where the spin excitation anisotropy for $BaFe_2As_2$ extends to much higher T/T_N than that of $SrFe_2As_2$. These results are qualitatively consistent with transport measurements of the resistivity anisotropy for $SrFe_2As_2$ and $BaFe_2As_2$.

III. DISCUSSION AND CONCLUSIONS

Theoretically, the electronic nematic phase and associated resistivity anisotropy is expected to only occur below the tetragonal-to-orthorhombic phase transition temperature T_s [11]. Although recent neutron pair distribution function and Larmor diffraction experiments on different classes of iron pnictides including $Sr_{1-x}Na_xFe_2As_2$ [35] and $NaFe_{1-x}Ni_xAs$ [36] reveal clear evidence for local orthorhombic lattice distortions in temperatures well above T_s, these local lattice distortions are evenly distributed along the two orthorhombic lattice directions and therefore not expected to induce resistivity anisotropy. The clear presence of resistivity [16,17], spin excitation [19–22], and orbital population anisotropy [37] in the paramagnetic phase of iron pnictides can arise from the interaction of applied uniaxial pressure with nematic susceptibility and associated spin excitations through magnetoelastic coupling [38]. The applied uniaxial pressure should be mostly sensitive to low-energy spin excitations and acoustic phonons, and have little impact on high-energy spin excitations. Since uniaxial pressure applied on the system has already broken the tetragonal symmetry of the paramagnetic phase, the system can only exhibit a paramagnetic to AF phase transition below T_N [30]. If nematic order in the paramgnetic phase of iron pnictides is driven by spin fluctuations associated with the static AF order [39,40], one would expect that the nature of the magnetic phase transition will affect critical spin fluctuations in the paramagnetic state near T_N. For systems with a strongly first-order AF phase transition, for instance $SrFe_2As_2$ [27,28], one would expect weak or no critical spin fluctuations associated with the magnetic order in the paramagnetic state. On the other hand, the AF phase transition in $BaFe_2As_2$ is a weakly first-order transition, and doping Co and Ni as well as uniaxial pressure drive the system into a second order AF phase transition [41–43]. Therefore, one would expect to find an extended critical regime and considerable critical magnetic scattering in the paramagnetic state.

By comparing the temperature dependence of the low energy spin excitation anisotropy of $BaFe_2As_2$ and $SrFe_2As_2$, we see a much faster reduction in spin excitation anisotropy in $SrFe_2As_2$, which is consistent with our transport measurements. Our experiments therefore establish a direct correlation between critical spin excitations in the paramagnetic state and resistivity anisotropy. Using the same reasoning, we would expect weak resistivity anisotropy and electronic nematic phase in the paramagnetic tetragonal phase of hole-doped iron pnictides $Ba_{1-x}K_xFe_2As_2$ [44] and isoelectronic doped $BaFe_2(As_{1-x}P_x)_2$ [45,46], since both materials have coupled first order structural and magnetic phase transitions. Indeed, transport measurements on uniaxial pressure detwinned $Ba_{1-x}K_xFe_2As_2$ reveal a much smaller region of resistivity anisotropy above T_N compared with similarly prepared electron-doped $BaFe_{2-x}Co_xAs_2$ [47]. On the other hand, since annealing as-grown single crystals of $BaFe_2As_2$ improves the first-order nature of the magnetic phase transition [48], reduces the disorder, resistivity anisotropy, and magnitude of residual resistivity [49,50], one would expect reduced spin-excitation anisotropy in the paramagnetic phase of annealed $BaFe_2As_2$. It would therefore be interesting to carry out studies of the annealing effect on the spin excitation anisotropy of $BaFe_2As_2$.

In summary, we have used transport and inelastic neutron scattering to study the effect of a strongly first-order magnetic phase transition on the magnitude and temperature dependence of resistivity and spin excitation anisotropy in the paramagnetic phase of $SrFe_2As_2$ and $BaFe_2As_2$. We find that the resistivity and spin excitation anisotropy in the paramagnetic state of iron pnictides are highly dependent on the nature of the magnetic phase transition. For $SrFe_2As_2$, a system with a first order magnetic phase transition, both the resistivity and spin excitation anisotropy disappear rapidly in the paramagnetic phase close to T/T_N due to a lack of critical spin fluctuations. For $BaFe_2As_2$, a system with a weakly first-order or second-order phase transition, the resistivity and spin excitation anisotropy extend to much higher T/T_N. These results are consistent with expectations of a spin excitation driven electronic nematic phase in the paramagnetic phase of iron pnictides, providing further evidence for the importance of magnetism to the electronic properties and superconductivity of iron based superconductors.

ACKNOWLEDGMENTS

The neutron-scattering work at Rice University was supported by the U.S. NSF Grant No. DMR-1700081 (P.D.). The $SrFe_2As_2$ single-crystal synthesis work at Rice University was supported by the Robert A. Welch Foundation Grant No. C-1839 (P.D.). Li Zhang was supported by the Natural Science Foundation of China (No. 61376094) and China Scholarship Council (No. 201408330028).

D.W.T. and W.W. contributed equally to this work.

[1] D. J. Scalapino, Rev. Mod. Phys. **84**, 1383 (2012).
[2] G. R. Stewart, Rev. Mod. Phys. **83**, 1589 (2011).
[3] P. C. Dai, Rev. Mod. Phys. **87**, 855 (2015).
[4] E. Fradkin, S. A. Kivelson, M. J. Lawler, J. P. Eisenstein, and A. P. Mackenzie, Annu. Rev. Condens. Matter Phys. **1**, 153 (2010).
[5] C. Fang, H. Yao, W.-F. Tsai, J. P. Hu, and S. A. Kivelson, Phys. Rev. B **77**, 224509 (2008).
[6] C. Xu, M. Müller, and S. Sachdev, Phys. Rev. B **78**, 020501(R) (2008).
[7] T. A. Maier and D. J. Scalapino, Phys. Rev. B **90**, 174510 (2014).
[8] M. A. Metlitski, D. F. Mross, S. Sachdev, and T. Senthil, Phys. Rev. B **91**, 115111 (2015).
[9] S. Lederer, Y. Schattner, E. Berg, and S. A. Kivelson, Phys. Rev. Lett. **114**, 097001 (2015).
[10] S. Lederer, Y. Schattner, E. Berg, and S. A. Kivelson, PNAS **114**, 4905 (2017).
[11] R. M. Fernandes, A. V. Chubukov, and J. Schmalian, Nat. Phys. **10**, 97 (2014).
[12] I. R. Fisher, L. Degiorgi, and Z. X. Shen, Rep. Prog. Phys. **74**, 124506 (2011).
[13] Q. Huang, Y. Qiu, Wei Bao, M. A. Green, J. W. Lynn, Y. C. Gasparovic, T. Wu, G. Wu, and X. H. Chen, Phys. Rev. Lett. **101**, 257003 (2008).
[14] M. G. Kim, R. M. Fernandes, A. Kreyssig, J. W. Kim, A. Thaler, S. L. Bud'ko, P. C. Canfield, R. J. McQueeney, J. Schmalian, and A. I. Goldman, Phys. Rev. B **83**, 134522 (2011).

[15] J. Zhao, W. Ratcliff, J. W. Lynn, G. F. Chen, J. L. Luo, N. L. Wang, J. P. Hu, and P. C. Dai, Phys. Rev. B **78**, 140504(R) (2008).
[16] J.-H. Chu, J. G. Analytis, K. De Greve, P. L. McMahon, Z. Islam, Y. Yamamoto, and I. R. Fisher, Science **329**, 824 (2010).
[17] J.-H. Chu, H.-H. Kuo, J. G. Analytis, and I. R. Fisher, Science **337**, 710 (2012).
[18] C. Dhital, Z. Yamani, W. Tian, J. Zeretsky, A. S. Sefat, Z. Wang, R. J. Birgeneau, and S. D. Wilson, Phys. Rev. Lett. **108**, 087001 (2012).
[19] X. Lu, J. T. Park, R. Zhang, H. Luo, A. H. Nevidomskyy, Q. Si, and P. Dai, Science **345**, 657 (2014).
[20] H. Man, X. Lu, J. S. Chen, R. Zhang, W. Zhang, H. Luo, J. Kulda, A. Ivanov, T. Keller, E. Morosan, Q. Si, and Pengcheng Dai, Phys. Rev. B **92**, 134521 (2015).
[21] W. Zhang, J. T. Park, Xingye Lu, Yuan Wei, Xiaoyan Ma, Lijie Hao, Pengcheng Dai, Zi Yang Meng, Yi-feng Yang, Huiqian Luo, and Shiliang Li, Phys. Rev. Lett. **117**, 227003 (2016).
[22] H. R. Man, R. Zhang, J. T. Park, X. Y. Lu, J. Kulda, A. Ivanov, and P. C. Dai, Phys. Rev. B **97**, 060507(R) (2018).
[23] R. M. Fernandes, E. Abrahams, and J. Schmalian, Phys. Rev. Lett. **107**, 217002 (2011).
[24] C. C. Lee, W. G. Yin, and W. Ku, Phys. Rev. Lett. **103**, 267001 (2009).
[25] F. Krüger, S. Kumar, J. Zaanen, and J. van den Brink, Phys. Rev. B **79**, 054504 (2009).
[26] W. C. Lv, J. S. Wu, and P. Phillips, Phys. Rev. B **80**, 224506 (2009).
[27] C. Krellner, N. Caroca-Canales, A. Jesche, H. Rosner, A. Ormeci, and C. Geibel, Phys. Rev. B **78**, 100504(R) (2008).
[28] A. Jesche, N. Caroca-Canales, H. Rosner, H. Borrmann, A. Ormeci, D. Kasinathan, H. H. Klauss, H. Luetkens, R. Khasanov, A. Amato, A. Hoser, K. Kaneko, C. Krellner, and C. Geibel, Phys. Rev. B **78**, 180504(R) (2008).
[29] S. D. Das, M. S. Laad, L. Craco, J. Gillett, V. Tripathi, and S. E. Sebastian, Phys. Rev. B **92**, 155112 (2015).
[30] Xingye Lu, Kuo-Feng Tseng, T. Keller, Wenliang Zhang, Ding Hu, Yu Song, Haoran Man, J. T. Park, Huiqian Luo, Shiliang Li, A. H. Nevidomskyy, and Pengcheng Dai, Phys. Rev. B **93**, 134519 (2016).
[31] X. Y. Lu, D. D. Scherer, D. W. Tam, W. L. Zhang, R. Zhang, H. Q. Luo, L. W. Harriger, H. C. Walker, D. T. Adroja, B. M. Andersen, and P. C. Dai, Phys. Rev. Lett. **121**, 067002 (2018).
[32] D. W. Tam, Y. Song, H. R. Man, S. C. Cheung, Z. P. Yin, X. Y. Lu, W. Y. Wang, B. A. Frandsen, L. Liu, Z. Z. Gong, T. U. Ito, Y. P. Cai, M. N. Wilson, S. L. Guo, K. Koshiishi, W. Tian, B. Hitti, A. Ivanov, Y. Zhao, J. W. Lynn, G. M. Luke, T. Berlijn, T. A. Maier, Y. J. Uemura, and P. C. Dai, Phys. Rev. B **95**, 060505(R) (2017).
[33] Y. C. Chen, X. Y. Lu, M. Wang, H. Q. Luo, and S. L. Li, Supercond. Sci. Technol. **24**, 065004 (2011).
[34] R. I. Bewley T. Guidi, and S. Bennington, Notiziario Neutroni e Luce di Sincrotrone **14**, 22 (2009).
[35] B. A. Frandsen, K. M. Taddei, D. E. Bugaris, R. Stadel, M. Yi, A. Acharya, R. Osborn, S. Rosenkranz, O. Chmaissem, and R. J. Birgeneau, Phys. Rev. B **98**, 180505(R) (2018).
[36] Weiyi Wang, Yu Song, Chongde Cao, Kuo-Feng Tseng, Thomas Keller, Yu Li, L. W. Harriger, Wei Tian, Songxue Chi, Rong Yu, A. H. Nevidomskyy, and Pengcheng Dai, Nat. Commun. **9**, 3128 (2018).
[37] M. Yi, Y. Zhang, Z.-X. Shen, and D. H. Lu, npj Quantum Mater. **2**, 57 (2017).
[38] Yu Li, Zahra Yamani, Yu Song, Weiyi Wang, Chenglin Zhang, D. W. Tam, Tong Chen, Ding Hu, Zhuang Xu, Songxue Chi, Ke Xia, Li Zhang, Shifeng Cui, Wenan Guo, Ziming Fang, Yi Liu, and Pengcheng Dai, Phys. Rev. X **8**, 021056 (2018).
[39] U. Karahasanovic and J. Schmalian, Phys. Rev. B **93**, 064520 (2016).
[40] M. H. Christensen, Jian Kang, B. M. Andersen, and R. M. Fernandes, Phys. Rev. B **93**, 085136 (2016).
[41] C. Lester, J.-H. Chu, J. G. Analytis, S. C. Capelli, A. S. Erickson, C. L. Condron, M. F. Toney, I. R. Fisher, and S. M. Hayden, Phys. Rev. B **79**, 144523 (2009).
[42] S. Nandi, M. G. Kim, A. Kreyssig, R. M. Fernandes, D. K. Pratt, A. Thaler, N. Ni, S. L. Bud'ko, P. C. Canfield, J. Schmalian, R. J. McQueeney, and A. I. Goldman, Phys. Rev. Lett. **104**, 057006 (2010).
[43] Xingye Lu, H. Gretarsson, Rui Zhang, Xuerong Liu, Huiqian Luo, Wei Tian, Mark Laver, Z. Yamani, Young-June Kim, A. H. Nevidomskyy, Qimiao Si, and Pengcheng Dai, Phys. Rev. Lett. **110**, 257001 (2013).
[44] S. Avci, O. Chmaissem, D. Y. Chung, S. Rosenkranz, E. A. Goremychkin, J. P. Castellan, I. S. Todorov, J. A. Schlueter, H. Claus, A. Daoud-Aladine, D. D. Khalyavin, M. G. Kanatzidis, and R. Osborn, Phys. Rev. B **85**, 184507 (2012).
[45] J. M. Allred, K. M. Taddei, D. E. Bugaris, S. Avci, D. Y. Chung, H. Claus, C. dela Cruz, M. G. Kanatzidis, S. Rosenkranz, R. Osborn, and O. Chmaissem, Phys. Rev. B **90**, 104513 (2014).
[46] Ding Hu, Xingye Lu, Wenliang Zhang, Huiqian Luo, Shiliang Li, Peipei Wang, Genfu Chen, Fei Han, S. R. Banjara, A. Sapkota, A. Kreyssig, A. I. Goldman, Z. Yamani, Christof Niedermayer, Markos Skoulatos, Robert Georgii, T. Keller, Pengshuai Wang, Weiqiang Yu, and Pengcheng Dai, Phys. Rev. Lett. **114**, 157002 (2015).
[47] J. J. Ying, X. F. Wang, T. Wu, Z. J. Xiang, R. H. Liu, Y. J. Yan, A. F. Wang, M. Zhang, G. J. Ye, P. Cheng, J. P. Hu, and X. H. Chen, Phys. Rev. Lett. **107**, 067001 (2011).
[48] C. R. Rotundu, B. Freelon, T. R. Forrest, S. D. Wilson, P. N. Valdivia, G. Pinuellas, A. Kim, J.-W. Kim, Z. Islam, E. Bourret-Courchesne, N. E. Phillips, and R. J. Birgeneau, Phys. Rev. B **82**, 144525 (2010).
[49] S. Ishida, T. Liang, M. Nakajima, K. Kihou, C. H. Lee, A. Iyo, H. Eisaki, T. Kakeshita, T. Kida, M. Hagiwara, Y. Tomioka, T. Ito, and S. Uchida, Phys. Rev. B **84**, 184514 (2011).
[50] S. Ishida, M. Nakajima, T. Liang, K. Kihou, C. H. Lee, A. Iyo, H. Eisaki, T. Kakeshita, Y. Tomioka, T. Ito, and S. Uchida, Phys. Rev. Lett. **110**, 207001 (2013).
[51] K. Matan, R. Morinaga, K. Iida, and T. J. Sato, Phys. Rev. B **79**, 054526 (2009).
[52] Chong Wang, Rui Zhang, Fa Wang, Huiqian Luo, L. P. Regnault, Pengcheng Dai, and Yuan Li, Phys. Rev. X **3**, 041036 (2013).
[53] J. Zhao, D.-X. Yao, S. Li, T. Hong, Y. Chen, S. Chang, W. Ratcliff II, J. W. Lynn, H. A. Mook, G. F. Chen, J. L. Luo, N. L. Wang, E. W. Carlson, J. Hu, and P. Dai, Phys. Rev. Lett. **101**, 167203 (2008).